Angewandte Chemie
Eine Zeitschrift der Gesellschaft Deutscher Chemiker

Supporting Information

Achieving Atomic Dispersion of Highly Loaded Transition Metals in Small-Pore Zeolite SSZ-13: High-Capacity and High-Efficiency Low-Temperature CO and Passive NO_x Adsorbers

*Konstantin Khivantsev, Nicholas R. Jaegers, Libor Kovarik, Jonathan C. Hanson, Franklin (Feng) Tao, Yu Tang, Xiaoyan Zhang, Iskra Z. Koleva, Hristiyan A. Aleksandrov, Georgi N. Vayssilov, Yong Wang, Feng Gao, and János Szanyi**

anie_201809343_sm_miscellaneous_information.pdf

Supporting Information

METHODS

Na-SSZ-13 with Si/Al = 6, 12 and 30 was hydrothermally synthesized and ion-exchanged twice with 2 M NH_4NO_3 aqueous solution at 80 °C for 3 hours yielding the ammonium forms of SSZ-13. NH_4-SSZ-13 was subsequently dried under ambient conditions and then at 80 ºC. Samples with 1-5 wt% Pd and 1 wt% Pt loadings were prepared by "modified ion exchange" (see below) with 10 wt% $Pd(NH_3)_4(NO_3)_2$ solution (Sigma-Aldrich 99.99%), palladium nitrate dihydrate (Sigma-Aldrich ≥ 99.9%) and platinum(II) tetraamine nitrate solution. More specifically, minimum amount of the Pd(II) or Pt(II) precursor solution was added to zeolite in the amount approximately equivalent to the total pore volume of the zeolite. The thick paste was mixed and stirred vigorously for 30 minutes, followed by calcination in air at 650 °C for 5 h (ramping rate 2 °C/min) in case of Pd and 350°C and 400°C in case of Pt. H-forms of zeolites could be used as well with identical results: in that case, Pd and Pt tetramine salts were dissolved in the minimum amount of dilute ammonium hydroxide solution (pH=11.5), mixed with zeolite to form thick paste (mixed vigorously), followed by drying and calcination in air at 650 °C for Pd and 350 °C for Pt.

When H-form of zeolites are used, Pd always agglomerates into PdO leading to underutilization of the expensive metal (Fig. S1)

How can we explain the low dispersion of Pd in this IWI-loaded H-from zeolites? In order for Pd ions to exchange with protons the following reaction has to take place:

$Pd(II) + 2\ Zeo\text{-}OH \leftrightarrow Zeo\text{-}(O)^2Pd + 2\ H^+$

This reaction is reversible. $Pd(OH)_2$ and $[Pd(OH)_4]^{2-}$ complexes are known to easily interact with H^+ with the formation of Pd(II) aqua complexes.[48] In the highly acidic environment inside the zeolite micropores, there is a competition for basic Zeo-O- sites between protons and Pd ions, and protons win this competition. As a consequence only a limited amount of metal cations ends up in ex-traframework positions when aqueous M(II) precursor solutions are mixed with H-from zeolites.[29-34] Thus, interaction of the metal precursor with H-form of a zeolite is not the right strategy to prepare such materials. The only other counter-ion that can be easily removed by heating, is ammonium. Indeed, exposure of NH_4-form of zeolites to metal cation-containing aqueous solutions leads to ion exchange. However, since it is an equilibrium reaction complete

ion exchange cannot be achieved. In some cases, multiple cycles of ion-exchange are required to shift the equilibrium toward the formation of metal zeolite with significant metal loadings. *How can this reaction be pushed to completion in one simple step?* It is possible if one of the products formed could be decomposed to gaseous compounds at low temperatures, thus shifting the equilibrium to the right in accordance with the Le-Chatelier principle. A similar principle is used, for example, for NH_3 decomposition. Due to a thermodynamic equilibrium, one cannot fully decompose NH_3 at normal high (>400 °C) operating temperatures: to push the equilibrium to the right, membranes are used that selectively remove the produced hydrogen gas.[48] Since we do not want to decompose the Pd-O-Zeolite, NH_4X salt has to decompose to gaseous products. One counter ion that can easily provide this is nitrate. NH_4NO_3 starts decomposing just above 180 °C, producing only gaseous N_2O and H_2O that are removed at this temperature.[49] With NH_4-SSZ-13, either $Pd(NO_3)_2$ or $[Pd(NH_3)_4](NO_3)_2$ thus is a viable option in this modified ion-exchange method. If one has to start with the H-form of zeolite, the Pd ammonia precursor should be dissolved in excess of ammonia solution with pH no higher than 11.5-12 and reacted with zeolite to form NH_4-zeolite in-situ.

The in situ static transmission IR experiments were conducted in a home-built cell housed in the sample compartment of a Bruker Vertex 80 spectrometer, equipped with an MCT detector and operated at 4 cm^{-1} resolution. The powder sample was pressed onto a tungsten mesh which, in turn, was mounted onto a copper heating assembly attached to a ceramic feedthrough. The sample could be resistively heated, and the sample temperature was monitored by a thermocouple spot welded onto the top center of the W grid. The cold finger on the glass bulb containing CO was cooled with liquid nitrogen to eliminate any contamination originating from metal carbonyls, while NO was cleaned with multiple freeze–pump–thaw cycles. Prior to spectrum collection, a background with the activated (annealed, reduced or oxidized) sample in the IR beam was collected. Each spectrum reported is obtained by averaging 256 scans.

HAADF-STEM was used to probe the dispersion of Pd in prepared samples. The analysis was performed with a FEI Titan 80-300 microscope operated at 300 kV. The instrument is equipped with a CEOS GmbH double-hexapole aberration corrector for the probe-forming lens, which allows for imaging with 0.1 nm resolution in scanning transmission electron microscopy

mode (STEM). The images were acquired with a high angle annular dark field (HAADF) detector with inner collection angle set to 52 mrad.

Standard NOx adsorption tests were conducted in a plug-flow reactor system with powder samples (120 mg, 60–80 mesh) loaded in a quartz tube, using a synthetic gas mixture that contained ~200 ppm of NOx or (200 ppm of NOx, 200 ppm CO, 3 vw% H_2O and 14% O_2) balanced with N_2 at a flow rate of 210 or 310 sccm (corresponding to 70,000 and 105,000 h^{-1}).

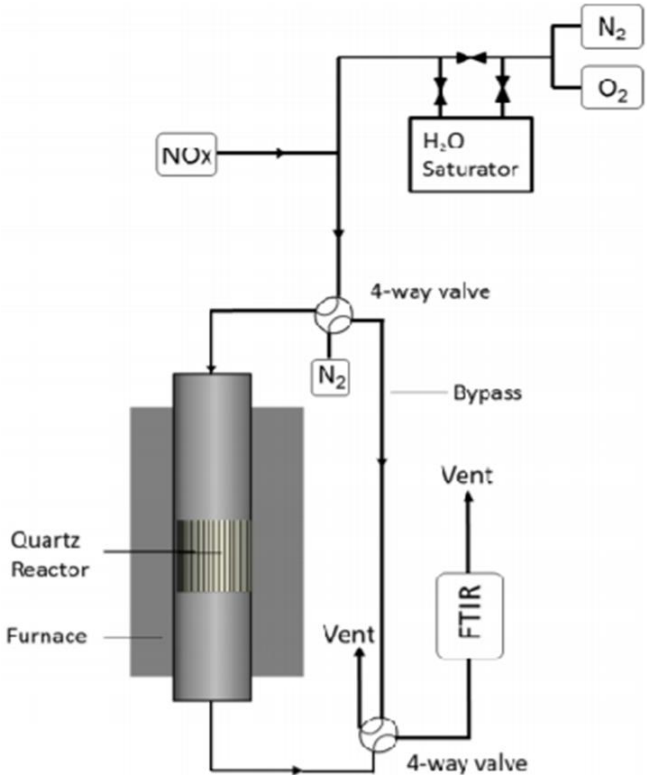

Note that to calculate GHSV we used industrially relevant powder density of the sample (which gives value 105,000 h^{-1}). Using real density of SSZ-13 (~2.1 g/cc) the GHSV value is ~330,000 h^{-1}. All the gas lines were heated to over 100 °C. Concentrations of reactants and products were measured by an online MKS MultiGas 2030 FTIR gas analyzer with a gas cell maintained at 191 °C. Two four-way valves were used for gas switching between the reactor and the bypass. Prior to storage testing at 100 °C, the sample was pretreated in 14% O_2 balanced in N_2 flow for 1 h at 550 °C and cooled to the target temperature in the same feed. The gas mixture was then switched from the reactor to the bypass, and 200 ppm of NOx was added to the mixture. Upon stabilization, the gas mixture was switched back from bypass to the reactor for storage testing for 10 min. The sample was then heated to 600 °C at a rate of 10 °C/min to record the desorption profiles of gases in the effluent.

XAS spectra were collected at X-ray beamline 4-1 of the Stanford Synchrotron Radiation Laboratory (SSRL), Stanford Linear Accelerator Center, Menlo Park, CA. The storage ring electron energy was 3 GeV and the ring current was in the range of 495-500 mA. Prior to these measurements, each powder sample was loaded into a wafer. The XAS data were collected in the transmission mode with a Si(220) double crystal monochromator that was detuned by 30% to minimize effects of higher harmonics in the X-ray beam. Samples were scanned at energies near the Pd *K* absorption edge (24,350 eV). All spectra were calibrated with respect to Pd foil or PdO reference, the spectrum of which was collected simultaneously.

The EXAFS data were analyzed with experimentally determined reference files obtained from EXAFS data references. The Pd–Pd and Pd–O contributions were analyzed with phase shifts and backscattering amplitudes obtained from EXAFS data for Pd foil and PdO, respectively.

Cryo High-energy X-ray Diffraction (XRD) data were collected at beamline 11-ID-B at the Advanced Photon Source at Argonne National Laboratory using 58.6 keV (0.2114 Å) X-rays. Samples were loaded in the powder form in low-background Kapton capillary holders, and cooled using liquid nitrogen microjets. Data were collected using amorphous silicon-based area detectors. Geometric corrections and reduction to one-dimensional data used GSAS-II.

Computational Details and Models

The calculations have been performed with density functional method with periodic boundary conditions. The PW91 exchange-correlation functional with dispersion correction (PW91-D2) [1,2] as implemented in the Vienna *ab initio* simulation package (VASP) [3,4] and ultrasoft pseudopotentials [5,6] have been used. The Brillouin zone was sampled using only the Γ point [7] since the simulation cell is large. The valence wave functions were expanded in a plane-wave basis with a cutoff energy of 400 eV.

The monoclinic unit cell of the CHA framework consists of 36 T atoms. It was optimized for the pure silicate structure with dimensions: a = b = 13.675 Å, c = 14.767 Å; $\alpha = \beta = 90^{o}$, $\gamma = 120^{o}$ [8]. Two Si atoms in the unit cell located in one six-member ring were replaced with Al. The negative charges around the Al sites were compensated by the Pd^{2+} ion or Pd^{+} and H^{+} cations or their complexes. During the geometry optimization procedure, all the zeolite atoms and the adsorbate species were allowed to relax until the force on each atom was less than 5×10^{-2} eV/Å. The total binding energy BE of all neutral ligands (CO, NO and H_2O) is calculated as follows:

$BE = E[ZEO/Pd(L1)_n(L2)_m] - E[ZEO/Pd] - n\times E(L1) - m\times E(L2)$

where $ZEO/Pd(L1)_n(L2)_m$ (n = 1, 2 or 3) is the energy of the optimized zeolite system together with the Pd cation and the adsorbed molecule(s); E[ZEO/Pd] are the energies of the pristine zeolite system, where the framework negative charges are compansated by Pd^+, H^+, $(PdH)^{2+}$, Pd^{2+}, $Pd^{2+}(OH)$, or $Pd^{2+}OPd^{2+}$ cations, while E(L1) and E(L2) are the energies of the adsorbate molecule(s) in the gas phase.

The adsorption energies of certain ligand (L1 or L2) in the Pd complexes $Pd(L1)_n(L2)_m$, (n=1-3, m = 0 - 2) located in the pores of chabazite zeolite are calculated as follows:

$BE_{L1} = E[ZEO/Pd(L1)_n(L2)_m] - E[ZEO/Pd(L1)_{n-1}(L2)_m] - E(L1)$

$BE_{L2} = E[ZEO/Pd(L1)_n(L2)_m] - E[ZEO/Pd(L1)_n(L2)_{m-1}] - E(L2)$

in the cases where there are two types of adsorbed ligands, L_1 and L_2 corresponds to the order of the ligands in the notation of the structure. For example in $Pd^{2+}(CO)(NO)$ structure CO is first ligand (L_1) and NO is the second one (L_2).

Consistent with these definitions, negative values of BE imply a favorable interaction.

The vibrational frequencies for periodic models were obtained from a normal mode analysis where the elements of the Hessian were approximated as finite differences of gradients, displacing each atomic center by 1.5×10^{-2} Å either way along each Cartesian direction. All calculated C-O vibrational frequencies were shifted by the difference of the calculated harmonic frequency of the free CO obtained with the same computational approach and the experimentally measured (anharmonic) frequency of CO in the gas phase (i.e., 2143 cm^{-1}):

$$\nu(C\text{-}O)^{calc} = \nu_{calculated} - \nu_{calculated}(CO\text{-}gas) + 2143.$$

In this case, the calculated ν_{CO} frequencies are corrected for both the anharmonicity (which is 35 cm^{-1} for gas phase CO) and the systematic error of the computational method. Such correction cannot be applied for the N-O vibrational frequencies due to the change in the oxidation state, when NO ligands are adsorbed to the Pd species.

References

[1]. J.P. Perdew, Y. Wang. Accurate and Simple Analytic Representation of the Electron-Gas Correlation Energy. *Phys. Rev. B* **1992**, *45*, 13244–13249.

[2]. Grimme, S. J. Comput. Chem. 2006, 27, 1787−1799.

[3]. G. Kresse, J. Hafner. Ab Initio Molecular-Dynamics Simulation of the Liquid-Metal-Amorphous-Semiconductor Transition in Germanium. *Phys. Rev. B* **1994**, *49*, 14251–14269.

[4]. G. Kresse, J. Furthmüller. Efficiency of Ab-Initio Total Energy Calculations for Metals and Semiconductors Using a Plane-Wave Basis Set. *Comput. Mater. Sci.* **1996**, *6*, 15–50.
[5]. D. Vanderbilt. Soft Self-Consistent Pseudopotentials in a Generalized Eigenvalue Formalism. *Phys. Rev. B* **1990**, *41*, 7892–7895.
[6]. G. Kresse, J. Hafner. Norm-Conserving and Ultrasoft Pseudopotentials for First-Row and Transition-Elements. *J. Phys.*: *Condens. Matter* **1994**, *6*, 8245–8257.
[7]. Y. Jeanvoine, J. Angyan, G. Kresse, J. Hafner. Bronsted Acid Sites in HSAPO-34 and Chabazite: An Ab Initio Structural Study. *J. Phys. Chem. B* **1998**, *102*, 5573–5580.
[8]. Ch. Baerlocher, L.B. McCusker. Database of Zeolite Structures. http://www.iza-structure.org/databases/.

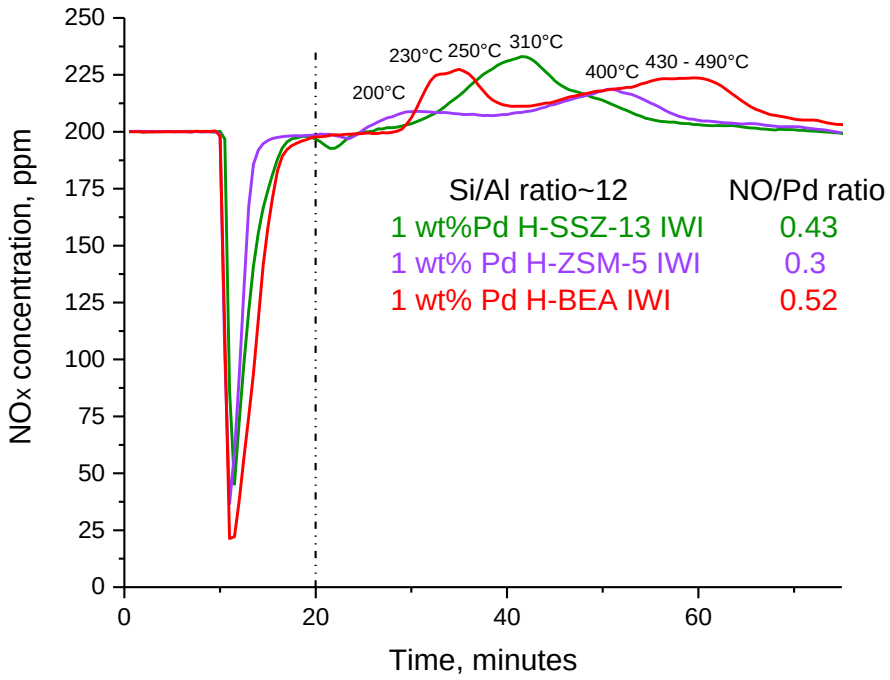

Figure S1. NOx adsorption at 100 °C for 10 min (after 10 min bypass) followed with TPD (10 °C/min). The feed gas mixture contains 200 ppm of NOx, 14% O_2, 3 % H_2O with 200 ppm CO

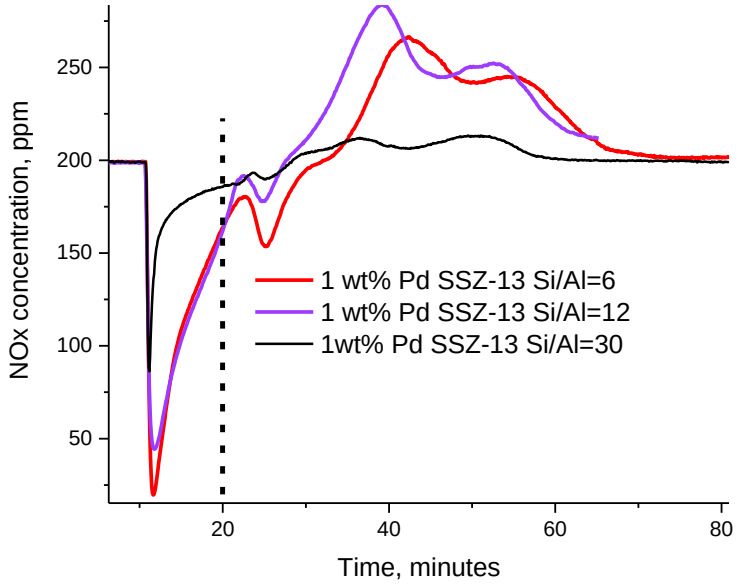

Figure S2. PNA performance of 1 wt% Pd SSZ-13 materials with different Si/Al ratios. NOx adsorption at 100 °C for 10 min (after 10 min bypass) followed with TPD (10 °C/min). The feed gas mixture contains 200 ppm of NOx, 200 ppm CO 14% O_2, 3 % H_2O.

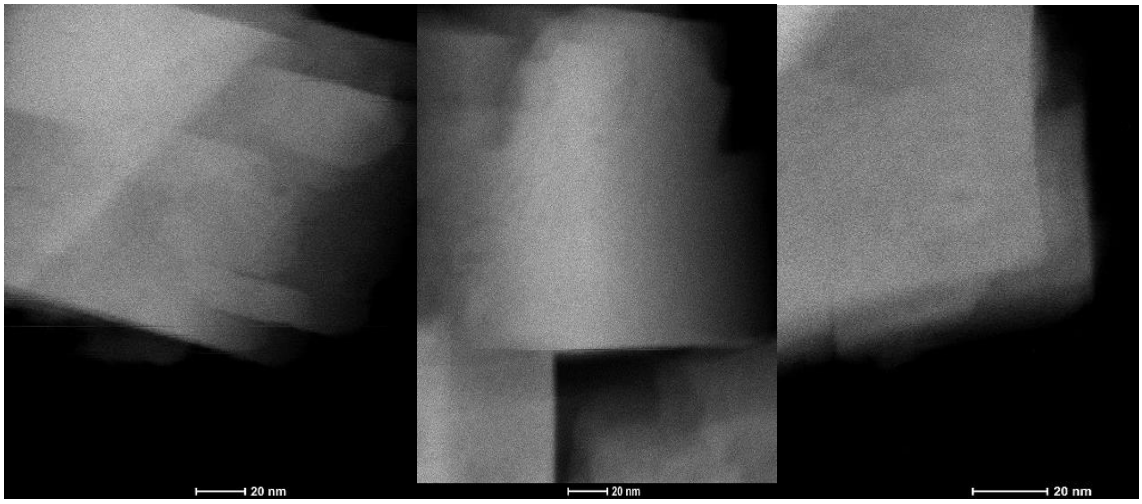

Figure S3. Additional HAADF-STEM images of 1 wt% Pd/SSZ13 with Si/Al ratio 6.

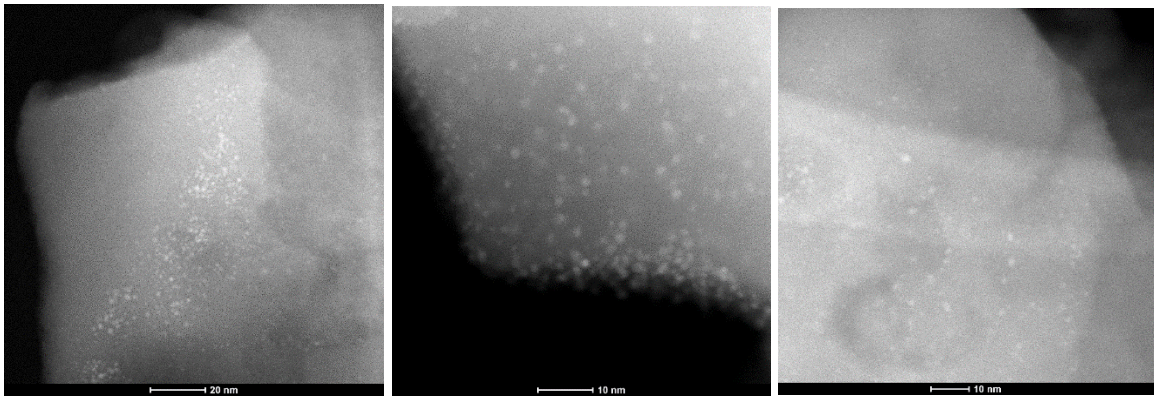

Figure S4. Additional HAADF-STEM images of 1 wt% Pd/SSZ13 with Si/Al ratio 12.

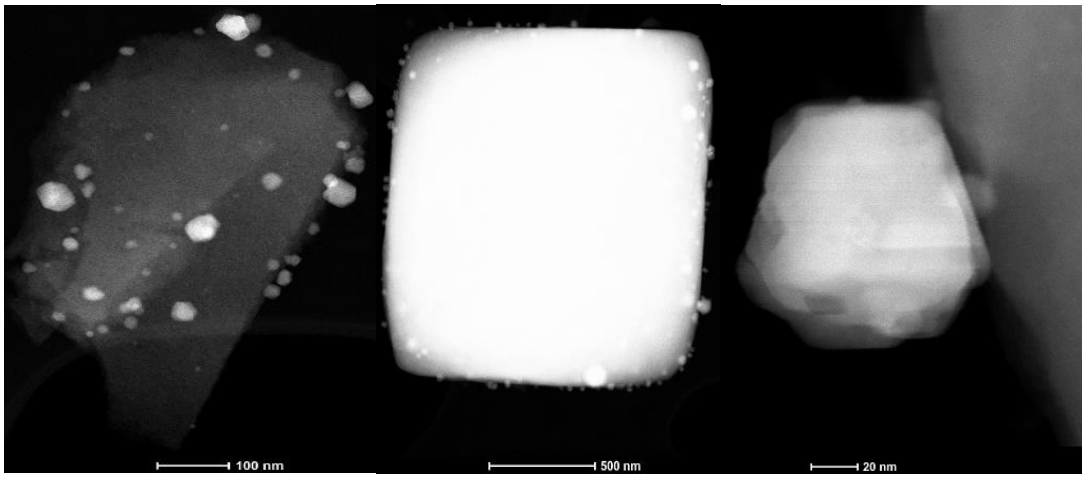

Figure S5. Additional HAADF-STEM images of 1 wt% Pd/SSZ13 with Si/Al ratio 30.

Table S1. Binding energies of the neutral ligands, in kJ/mol (calculated as described in computational details), vibrational frequencies of diatomic ligands (υ(L) in cm^{-1}), elongation of the bond length(s) in the ligands with respect to isolated molecule in gas phase, Pd-ligand and Pd-O_{zeo} distances (in pm), and number of the unpaired electrons in the systems, N_s.

Structures	BE	BE_{L1}	BE_{L2}	υ(L)[a]	Δd(A-B)[b]	d(Pd-L)	d(Pd-O_{zeo})	N_s
Pd^+							220;222;225	1
$Pd^{3+}H_{zeo}$	85[c]					149	215;217;224;227	1
$Pd^+(NO)$	-226			1804	0.3	181	220;231	0
$Pd^+(CO)$	-158			2075	1.1	188	214;246;258	1
$Pd^+(CO)_2$	-252	-94		2103;2063	0.5;0.7	195;197	224;235	1
Pd^{2+}							206;206;214;214	0
$Pd^{2+}(CO)$	-87			2114	0.4	188	206;213;214	0
$Pd^{2+}(CO)_2$	-215	-128		2172;2138	-0.2;-0.2	192;192	210;210	0
$Pd^{2+}(NO)$	-122			1843	-1.1	193	218;219;232;233	1
$Pd^{2+}(NO)_2$	-243	-121		1879;1823	0.1;0.8	197;201	223;235	0
$Pd^{2+}(CO)(NO)$	-200	-78	-113	2146/1830	-0.1/-1.1	193/199	213;217	1
$Pd^{2+}(CO)(NO)_2$	-319	-50	-232	2148/1852;1808	-0.3/-1.2;-1.1	199/215;215	232;238;238	0
$Pd^{2+}(CO)(OH)$[e]		-187		2121	0.4/-0.1[g]	187/198	213;219	0
$Pd^{2+}(H_2O)$[h]	-50				0.5;7.2	206	203;215;217	0
$Pd^{2+}(CO)(H_2O)$[i]	-209	-159	-122	2148	-0.1/0.7;8.0	188/209	209;210	0
$Pd^{2+}(O)Pd^{2+}$							214;219/214;219	0
$Pd^{2+}(CO)(O)Pd^{2+}(CO)$	-321			2132/2116	0.3/0.3	188/188	214;219/214;219	0
$Pd^{2+}(CO)_2(O)Pd^{2+}(CO)_2$	Spontaneous formation and desorption of CO_2							

[a] shifted by +35 cm^{-1} since the calculated CO in gas phase 2108 cm^{-1} is lower by 35 cm^{-1} with respect to the experimental value, 2143 cm^{-1}; the calculated frequencies of NO are not shifted.

[b] elongation with respect to the isolated ligand

[c] relative energy with respect to Pd^+ structure

[g] elongation of OH with respect to Pd^{2+}(OH)/zeo complex

Hydrogen bond between the H from OH and O from the zeolite: [e] 204 pm.

Hydrogen bond between the H from H_2O and O from the zeolite: [h]147.8 pm; [i] 149.0 pm.

Table S2. Comparison of different PNA materials. *Note that no other PNA material except the ones reported in this work, were highlighted to abate CO effectively in addition to NOx at low temperature. References are provided in the main text of the manuscript.*

Material	NOx storage	NO/Pd ratio
1 wt% Pd/SSZ-13 Si/Al=11[38,39]	48 µmoles/g	0.5
1 wt% Pd/ZSM-5 Si/Al=12[38,39]	55 µmoles/g	0.6
1 wt% Pd/BEA Si/Al=14[38,39]	65 µmoles/g	0.68
2 wt% Pd/SSZ-13 Si/Al=22[45]	26 µmoles/g	N/A
2 wt% Pd/ZSM-5 Si/Al=22[45]	24 µmoles/g	N/A
1 wt% Pd/BEA Si/Al=25[44]	20 µmoles/g	0.2
Pd/Pt on various Alumina, Ceria and Ceria-Zirconia supports[35,36,40,43]	10-30 µmoles/g	N/A
1 wt% Pd/SSZ-13 Si/Al=6[this work]	94 µmoles/g	1
1.9 wt% Pd/SSZ-13 Si/Al=6[this work]	180 µmoles/g	1
3 wt% Pd/SSZ-13 Si/Al=6[this work]	250 µmoles/g	0.9

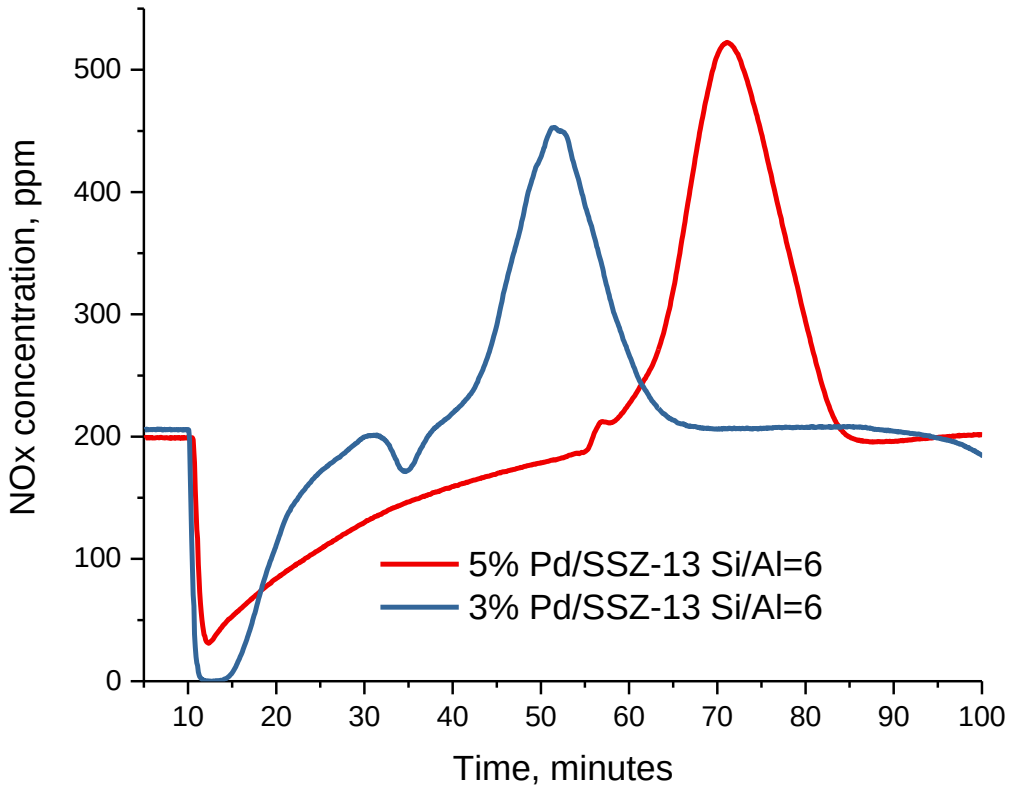

Figure S6. PNA performance of 3 wt% and 5 wt% Pd SSZ-13 with Si/Al ratio 6. NOx adsorption at 100 °C (after 10 min bypass) followed with TPD (10 °C/min). The feed gas mixture contains 200 ppm of NOx, 14% O_2, 3 % H_2O with 200 ppm CO. Note that for 3 and 5 wt% Pd/SSZ-13 TPD was started at ~30 and 50 minute mark correspondingly.

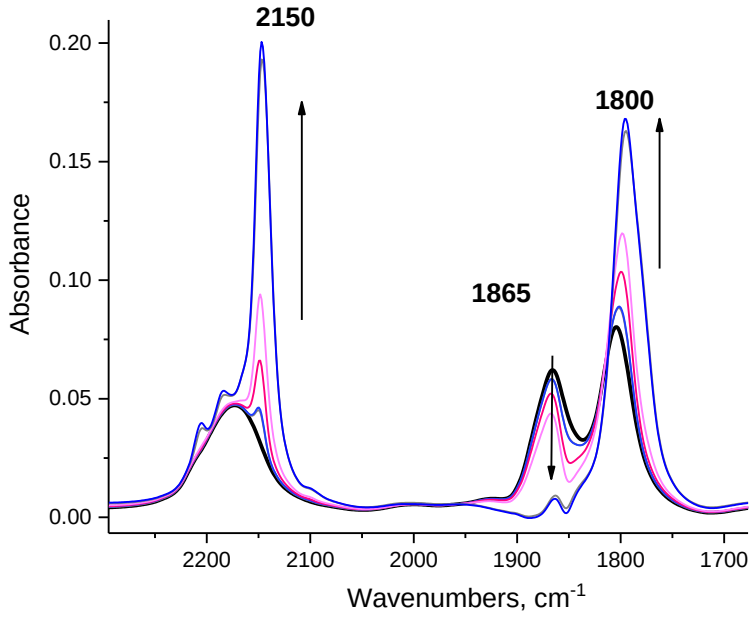

Figure S7. FTIR spectra collected during step-wise addition of 0.5 Torr CO adsorption on an NO saturated 1wt% Pd/H-SSZ-13 sample. Final pressure 0.02 Torr.

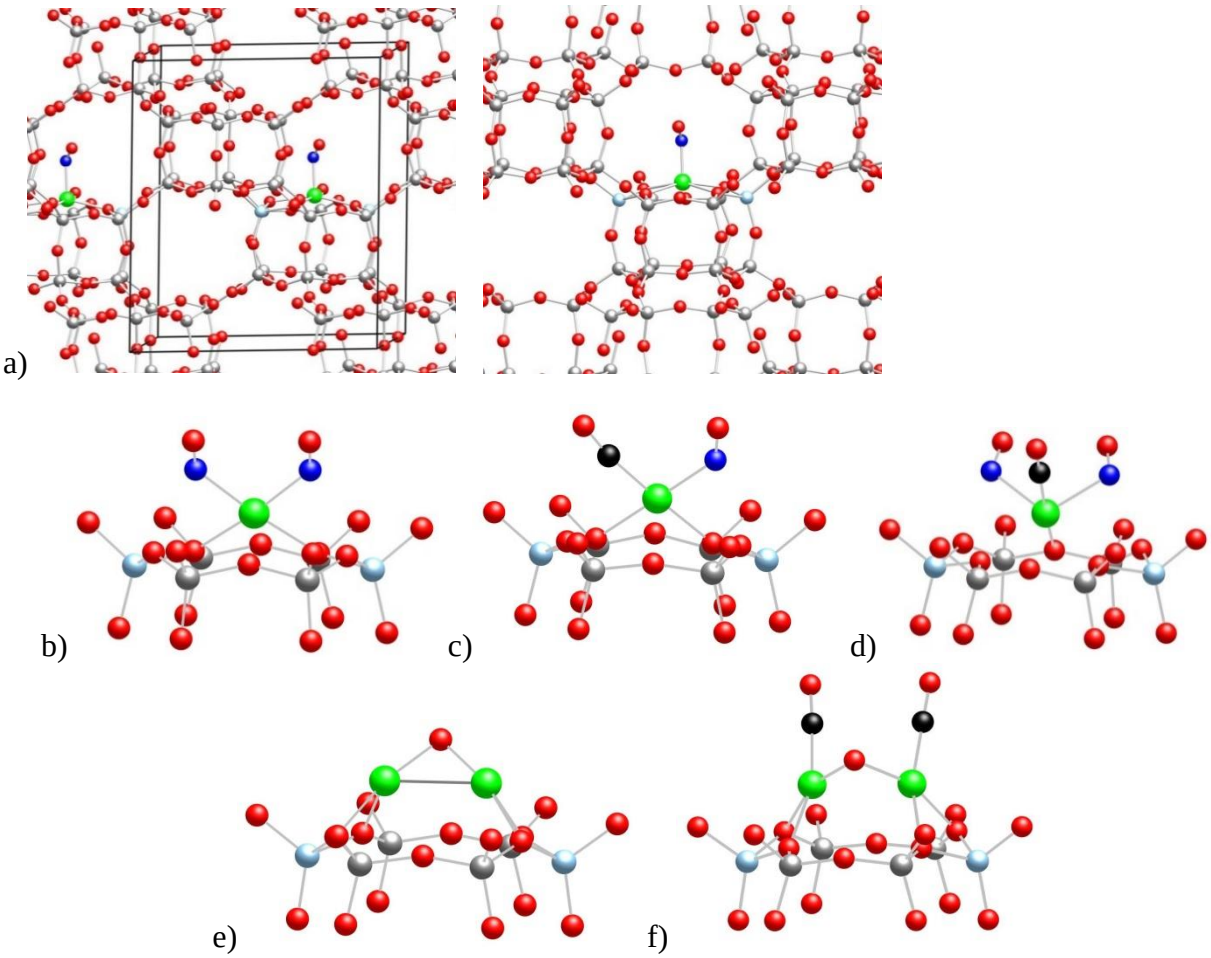

Figure S8. Optimized structures of selected complexes: (a) different views of the location of the complexes in the cavity of the chabazite framework, represented by $Pd^{2+}(NO)$ complex; local structure of: (b) $Pd^{2+}(NO)_2$; c) $Pd^{2+}(CO)(NO)$; d) $Pd^{2+}(CO)(NO)_2$ complexes. Structures with $Pd^{2+}(O)Pd^{2+}$ dimer: e) pristine dimer; f) $Pd^{2+}(CO)(O)Pd^{2+}(CO)$. Color coding: Si – gray; O – red; Al – light blue; C – black; N – blue; Pd – green.

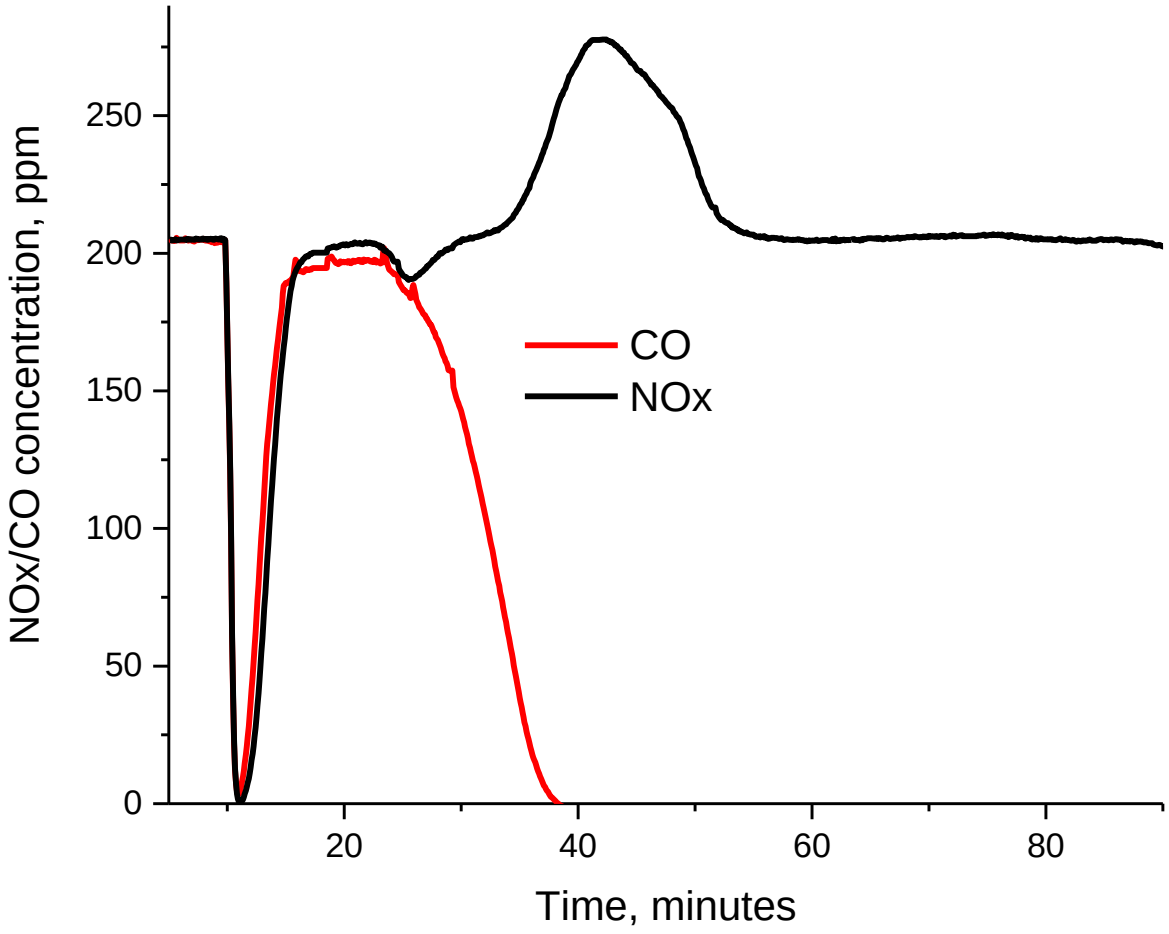

Figure S9. NOx and CO abatement performance of 1 wt% Pd SSZ-13 with Si/Al = 6. NOx adsorption at 100 °C for 10 min (after 10 min bypass) followed with TPD (10 °C/min). The feed gas mixture contains 200 ppm of NOx, 14% O_2, 3 % H_2O with with 200 ppm CO.

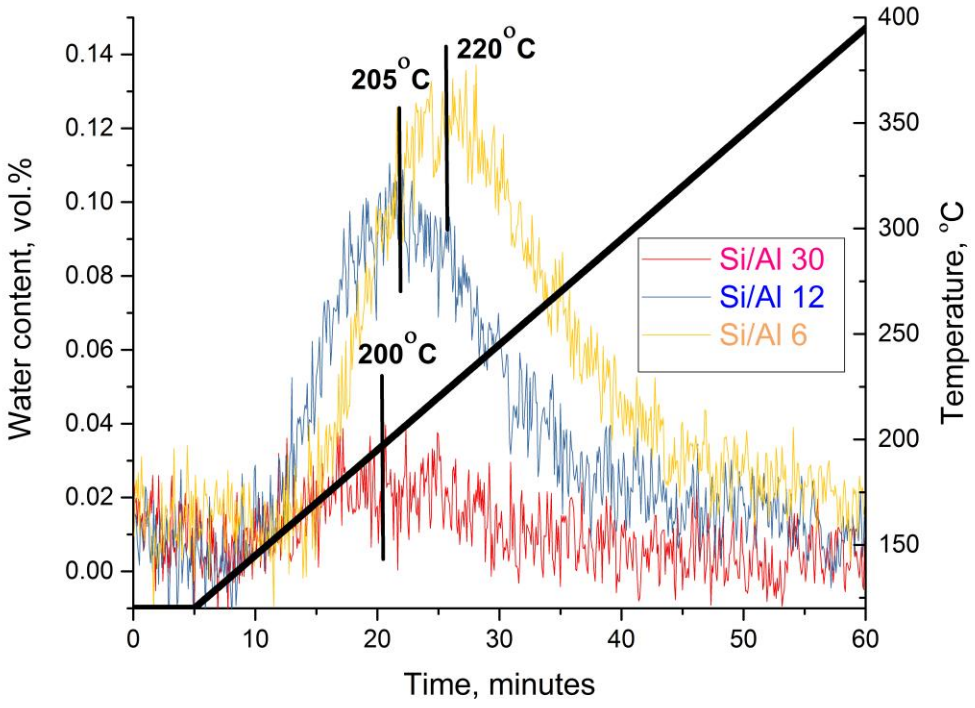

Figure S10. H_2O Temperature Programmed Desorption (TPD) on H-SSZ-13 materials with Si/Al of 6, 12 and 30: the samples (120 mg) was saturated with H_2O/N_2 vapor at 120 ºC, then purged with N_2 for 3 hrs and TPD was started at 5 minute mark at 5 ºC/min.

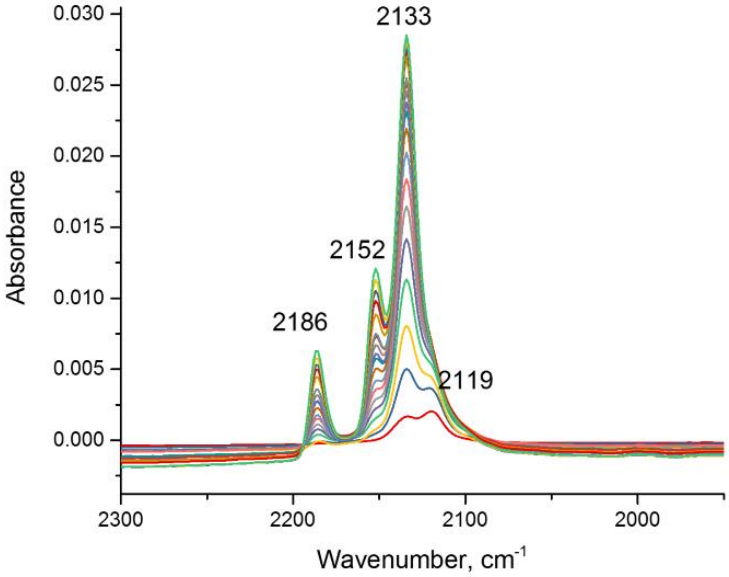

Figure S11. Series of FTIR spectra recorded at 20 ºC during 5 Torr CO adsorption on 1 wt% Pt/SSZ-13 with Si/Al = 6

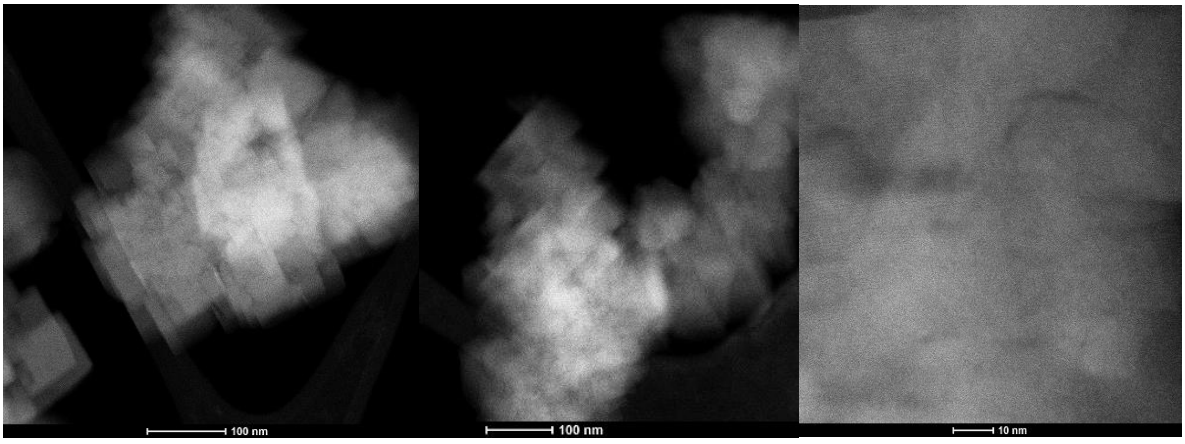

Figure S12. Additional HAADF-STEM images of different crystals/areas of 1 wt% Pt/SSZ13 with Si/Al ratio 6.

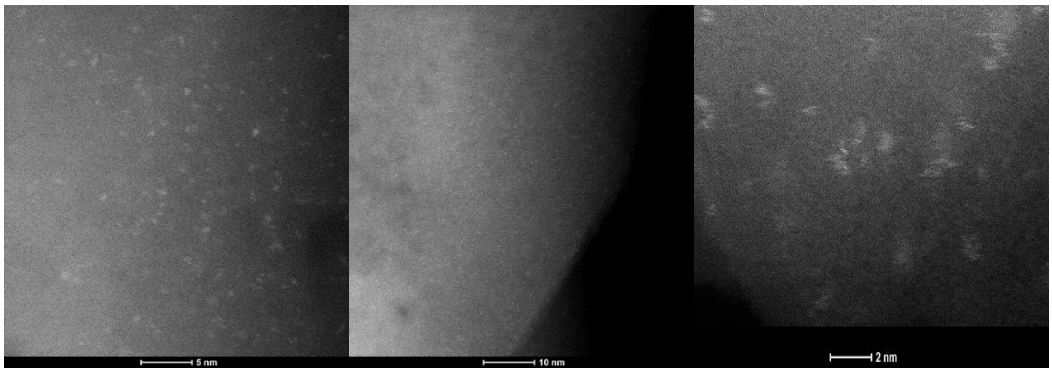

Figure S13. Additional HAADF-STEM images of 1 wt% Pt/SSZ13 with Si/Al ratio 6, showing that in beam-damage parts of the sample (framework gets damaged quickly under the electron beam) small Pt clusters are observed.

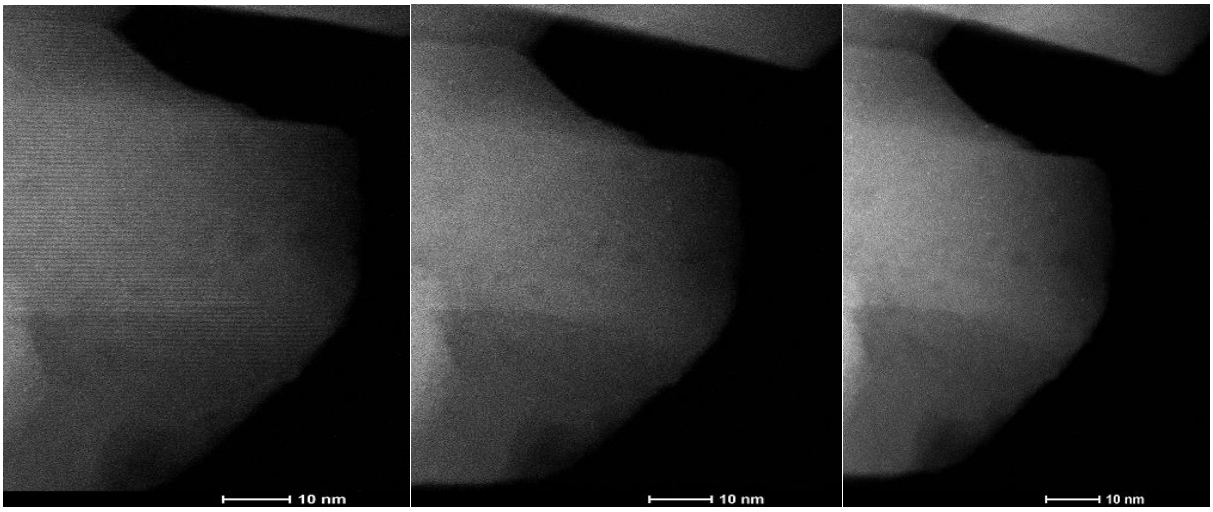

Figure S14. Sequential HAADF-STEM images of 1 wt% Pt/SSZ13 with Si/Al ratio 6, showing (in addition to Figure 5 in the main text) that initially (before the beam damage) all Pt is atomically dispersed. Under the beam, within seconds, the framework starts to amorphize and Pt clusters start to appear as a consequence

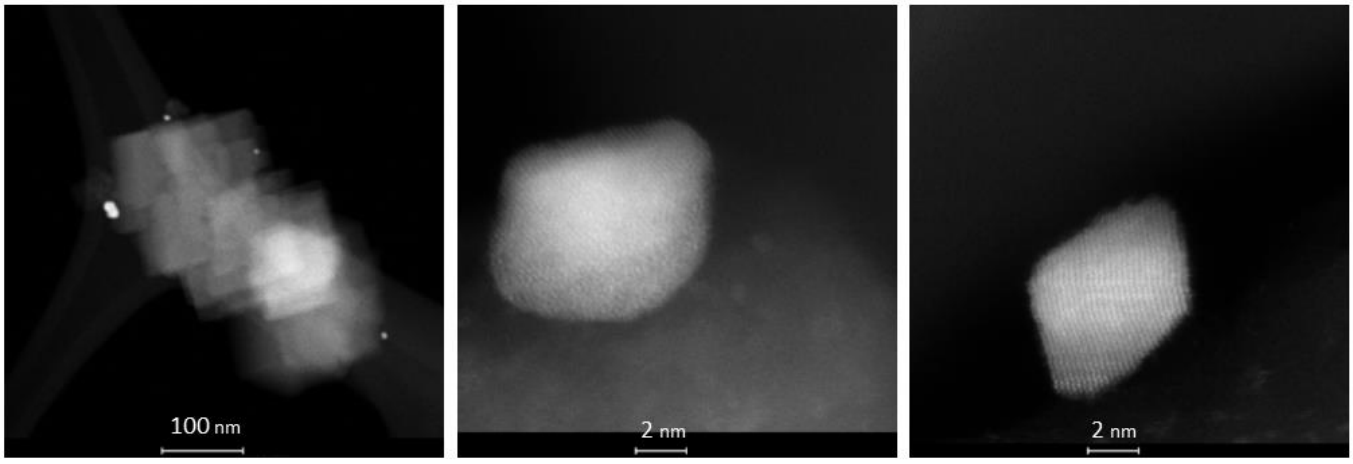

Figure S15. HAADF-STEM images of 1 wt% Pt/SSZ13 with Si/Al ratio 6 calcined in air at 400 ºC showing formation of metallic Pt on the external surface of SSZ-13.

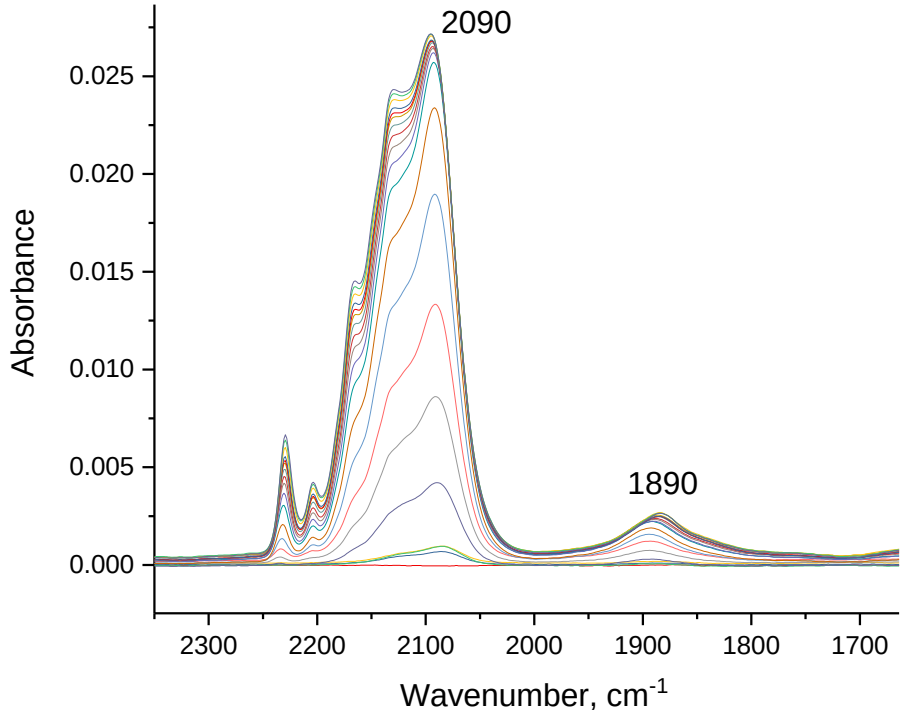

Figure S16. CO adsorption (5 Torr, 20 ºC) on 1 wt% Pt/H-SSZ-13 (Si/Al = 6) that was calcined in oxygen at 400 ºC. 2090 and 1890 cm^{-1} bands belong to metallic Pt.

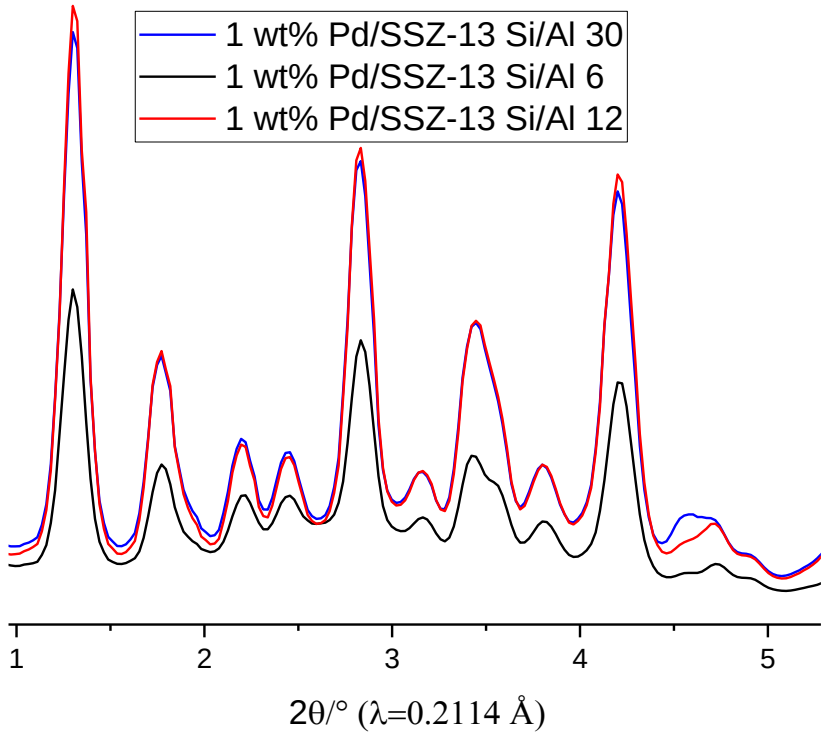

Figure S17. High-energy cryo-XRD of 1 wt% Pd/SSZ13 with different Si/Al ratios